The Cryosphere Discuss., https://doi.org/10.5194/tc-2017-111
Manuscript under review for journal The Cryosphere
Discussion started: 14 July 2017

The Cryosphere Discussions
Open Access
EGU

Black carbon and mineral dust in snow cover on the Third Pole

Yulan Zhang[1], Shichang Kang[1,2*], Michael Sprenger[3], Zhiyuan Cong[2], Tanguang Gao[4], Chaoliu Li[2], Shu Tao[5], Xiaofei Li[1], Xinyue Zhong[1], Min Xu[1], Wenjun Meng[5], Mika Sillanpää[6]

[1]State key laboratory of Cryospheric Sciences, Northwest Institute of Eco-Environment and Resources, Chinese Academy of Sciences, Lanzhou730000, China
[2]CAS Center for Excellence in Tibetan Plateau Earth Sciences, Beijing 100101, China
[3]Institute for Atmospheric and Climate Science, ETH Zurich, CH-8092 Zurich, Switzerland
[4]Key Laboratory of Western China's Environmental System (Ministry of Education), College of Earth and Environmental Sciences, Lanzhou University, Lanzhou 730000, China
[5]Department of Environmental Science, Laboratory for Earth Surface Processes, Peking University, Beijing, China
[6]Laboratory of Green Chemistry, Lappeenranta University of Technology, Mikkeli 50130, Finland

Correspondence to: Prof. Shichang Kang (shichang.kang@lzb.ac.cn)

Abstract. Light-absorbing impurities (including black carbon, organic carbon, and mineral dust) deposited on snow can reduce surface albedo and contribute to the near-worldwide melting of snow cover and ice. This study found that the black carbon, organic carbon, and dust concentrations in snow cover ranged generally from 202–17468 ng g^{-1}, 491–13880 ng g^{-1}, and 22–846 μg g^{-1}, respectively, with higher concentrations in the central to northern areas of the Third Pole region (referred to by scientists also as the Tibetan Plateau and its surrounding mountains). Footprint analyses suggested that the northern Third Pole was influenced mainly by air masses from Central Asia with some Euro-Asia influence; air masses in the central and Himalayan region originated mainly from Central and South Asia. The open burning-sourced black carbon contributions decreased from ~50 % in the southern Third Pole region to ~30 % in the northern Third Pole region. The contribution of black carbon and dust to snow albedo reduction reached approximately 37% and 15 %, respectively. The effect of black carbon and dust reduced the average snow cover duration by 3.1 ±0.1 days to 4.4 ±0.2 days. Meanwhile, the black carbon and dust had an import implication for snowmelt water loss over the Third Pole region. Findings indicate that the impacts of black carbon and mineral dust need to be properly accounted for in future regional climate projections, particularly in the high-altitude cryosphere.

1 Introduction

Black carbon (BC), organic carbon (OC), and mineral dust (MD) are the main constituents of light-absorbing impurities (LAIs) in snow (Andreae and Gelencsér, 2006; Bond et al., 2013; Mauro et al., 2015; Painter et al., 2010). LAIs can reduce snow and ice albedo and trigger positive feedbacks that contribute to the near-worldwide melting of snow cover and ice (Flanner et al., 2007; Hadley and Kirchstetter, 2012; Hansen and Nazarenko, 2004; Painter et al., 2013). As a result of its absorption of solar radiation, BC is now considered to be the second most important climate forcer in the present climate system only after carbon dioxide (Bond et al., 2013). Model studies in the recent decades indicate that BC in seasonal snow may be responsible for a

significant impact on warming and albedo reduction over the Arctic (Flanner, 2013; Qian et al., 2014), Greenland (Dumont et al., 2014), Alps (Painter et al., 2013; Yasunari et al., 2015), and the Third Pole region (He et al., 2014; Jacobi et al., 2015; Ji et al., 2015; Ménégoz et al., 2014). The snow albedo feedback of BC may also be an important driver accelerating glacial retreat and snow cover melt (Painter et al., 2013; Xu et al., 2009).

Light-absorbing OC in snow can contribute significantly to the absorption by ultraviolet/visible light (Andreae and Gelencsér, 2006). Bahadur et al. (2012) Studied aerosol optical properties derived from Aerosol Robotic Network (AERONET) measurements and estimated that, in California, OC absorption at 440 nm was approximately 40 % of the BC absorption. Measurements of hundreds of snow samples revealed that about 40 % of the light absorption from impurities in Arctic snow and sea ice is due to non-BC constituents (Doherty et al., 2010). In western North America, Dang and Hegg (2014) suggested that OC was responsible for more than 10 % of the total light absorption (Dang and Hegg, 2014). A global model by Lin et al. (2014) estimated the role of OC in the reduction of snow albedo; the simulation showed that the radiative forcing (RF) of OC deposited in land snow and sea ice ranges from +0.0011 to +0.0031 W m^{-2} or as large as 24 % of the forcing caused by BC in snow and ice.

MD, an important LAI component in snow cover (Mauro et al., 2015; Painter et al., 2010, 2013; Skiles et al., 2015), can change the cryospheric environment and hydrological cycle due to its light-absorbing properties (Ji et al., 2016a; Painter et al., 2007). In the San Juan Mountains of the USA, a seasonal snow covered range, snow cover duration was found to be shortened by 18 to 35 days during ablation through surface short-wave RF caused by deposition of disturbed desert dust (Painter et al., 2007). In a study of two sites on Claridenfirn of Swiss Alps, Gabbi et al. (2015) showed that the mineral dust lowered the mean annual albedo by 0.006–0.011, depending on the location on the glacier, causing a reduction of approximately 142–271 mm in annual mass balance. Confirming radiative transfer modelling, a study of the Mera glacier on the southern slope of the Himalayas indicated that, when dust concentrations are high, dust dominates absorption, snow albedo reduction, and RF, and the impact of BC may be negligible (Kaspari et al., 2014).

As an important component of the hydrology, snow cover plays a key role for sustaining ecology and society in mountainous regions (Beniston et al., 2017). Snowpack changes are not only crucial to estimate impacts on water resource, but also to anticipate natural hazards related to snow avalanches/disasters (Beniston et al., 2017; Brown and Mote, 2009). Covered by a large volume of snow/ice in the mid-low latitudes, the Third Pole (TP, also known as the Tibetan Plateau) is the most sensitive and readily visible indicator of climate change (Yao et al., 2012a). Recently, the TP cryosphere has undergone rapid changes (Kang et al., 2010), including glacial shrinkage (Yao et al., 2012b), permafrost degradation (Cheng and Wu, 2007), and reduction in the annual duration of snow cover by 1 to 8 days (Ménégoz et al., 2014). Studies on the TP indicate that BC has been a significant contributing factor to the observed cryospheric change (Li et al., 2017; Ming et al., 2009; Niu et al., 2017; Xu et al., 2009;Yang et al., 2015), and a major forcer of climate change (Qian et al., 2015; Ji, 2016a). Observations and simulations also found that MD deposition on snow/ice can change the surface albedo and result in perturbations in the surface radiation balance (Ji et al., 2016b; Qu et al., 2014), causing a decrease of 5–25 mm in the snow water equivalent over the western TP and Himalayas (Ji et al., 2016b). .

Snowpack on the TP is associated with the Asian summer monsoon, and is a crucial water source for several major rivers of Asia (Lau et al., 2010; Vernekar et al., 1995; Yao et al., 2012a). Atmospheric heating related to BC and MD deposition can lead to widespread enhanced warming over the TP and accelerated snowmelt in the western TP and Himalayas (Lau et al., 2010; Ramanathan and Carmichael, 2008; Zhang et al., 2015). Simulation studies of BC in snow over the TP have inherent uncertainties because of the lack of large-area observations of BC data in seasonal snow cover (Gertler et al., 2016; Yasunari et al., 2010, 2013). For example, Kopacz et al. (2011) estimated RF of 5 to 15 W m^{-2} due to BC within the snow-covered areas of Himalaya and TP, while Flanner et al. (2007) and Qian et al. (2011) estimated peak values of BC effects exceeding 20 W m^{-2} for some parts of the TP. Menon et al. (2010) and Ménégoz et al. (2014) proposed that during the last decade BC in snow caused a significant part of the decrease of the snow cover extent or duration observed in the TP during the last decade. Ji et al. (2016b) found a positive surface RF was induced by MD, which caused a decrease of 5–25 mm in the snow water equivalent (w.e.) over the western TP, Himalayas, and Pamir Mountains from December to May.

To further understand the role of BC and other water-insoluble LAIs in TP snowpack, more measurements and an extended LAI dataset of snow cover properties is needed to validate and calibrate models. This study is an attempt to fill that gap. Snow cover samples were collected across the TP in winter seasons (Table S1 and S2), which will provide the first large-area survey of BC and dust in seasonal snow cover over the TP, investigate albedo reduction and RF, and estimate changes in snow cover duration caused by LAIs. Footprint analysis coupling with BC emission inventory is to constrain different BC source contributions. The results of this study will increase understanding of BC and other LAIs in snow cover across the TP and enable improved climate modeling.

2 Methodology

2.1 Study area

The TP covers an area of 5 million km^2 with an average elevation greater than 4000 m a.s.l. (Yao et al., 2012a). The TP exerts profound influences on atmospheric circulation and climate through mechanical and thermal effects because of its large area, unique topography, and geographical location in the earth system (Yanai and Wu, 2006). Extended glacier coverage (over 100,000 km^2) and snow cover have the potential to modify regional hydrology and trigger natural hazards that can impact local populations, agriculture, and water resources in and around the region (e.g., Immerzeel et al., 2010; Xu et al., 2009; Yao et al., 2012a).

Moderate Resolution Imaging Spectroradimeter (MODIS) snow cover data from 2000–2006 showed that the spatial distribution of snow cover is quite variable over the TP because of the complex terrain (Pu et al., 2007). Maximum snow accumulation and melting times vary over the year, but are generally later as the elevations increases. Additionally, large interannual variabilities occur in the late autumn and winter months. Heating by light-absorbing aerosols produces an atmospheric dynamical feedback, which increases moisture, cloud cover, and deep convection over northern India, and enhances the rate of snow melt in the Himalayas and TP (Lau et al., 2010; Ramanathan and Carmichael, 2008). The accelerated

melting of snow is confined mostly to the western TP, beginning slowly in early April and then progressing more rapidly from early to mid-May; the snow cover remains reduced from mid-May through early June (Lau et al., 2010). The decadal change in the spring snow depth over the TP can impact on the Asian summer monsoon and a close relationship exists between the interdecadal increase of snow depth over the TP during March–April, increased summer rainfall over the Yangtze River valley, and a dryer summer along the southeast coast of China and the Indochina peninsula (Zhang et al., 2004).

2.2 Sample collection

For this study, snow cover samples were collected at 37 sites (Fig. 1a) and one river basin (Laohugou region, including 10 sites as in Fig. 1b) cross the TP in December 2014 and November 2015 (Table S1). As shown in Figure 1a, these field campaigns can be grouped into three regions, as was done in previous studies (Yao et al., 2013). Region I (Southern TP) includes 27 sites, and is dominated by the Indian monsoon. Region II (Central TP) contains 10 sites that are affected by both the westerlies and the Indian monsoon. Region III has one site (LHG) is located in the northeastern part of the TP. Seasonal snow samples (34) were also collected from the 10 sites in the LHG region of the Qilian Mountain (Fig. 1b) from December 2015 to June 2016.

To minimize the effects of local sources, we selected sampling sites more than 1 km away from roads and usually 30 km from villages and cities. Generally, snow samples were collected from the top 5 cm with cleaned stainless steel utensils, and placed in Whirl-Pak® bags. These snow samples were kept frozen until they underwent filtration. During sampling, snow depth, grain size, density and temperature were also observed. For the selected sites, a general-purpose spectroradiometer (FieldSpec 4, ASD, Inc.), was used to measure the reflectance of snow cover. The FieldSpec 4 instrument is a compact, field-portable and precision instrument with a spectral range of 350–2500 nm and has a rapid data collection time of 0.2 seconds per spectrum.

2.3 LAIs measurements

In the laboratory, the snow samples were melted rapidly in a hot-water bath to minimize the melt time. Immediately after melting, snow samples were filtered through pre-baked quartz filters (Whatman) using an electric pump to create a partial vacuum. Then sample meltwater was saved into polyethylene bottles, and refrozen for chemical analysis.

Because the mineral dust mass is much larger than BC and OC mass in snow samples compared to aerosol samples (Wang et al., 2012), dust concentrations were calculated by taking the difference in the weight of the quartz filter before and after filtration. Quartz filters were then used to analyze BC and OC with a thermal-optical carbon analyzer (DRI 2001A model, Desert Research Insitute, NV, USA) following a methodology (IMPROVE_A protocol) used in previous studies (Cao et al., 2003; Chow et al., 2004; Xu et al., 2009; Yang et al., 2015). Its function relies on the fact that OC components can be volatilized from the sample deposited in a non-oxidizing helium atmosphere, which BC can be combusted with oxidizer. The sample punch is palced in a quartz holder oriented to the dierection of the carrier gas flow, and heated gradually to a special temperature (typically 550 or 850 ℃) in a pure helium atmosphere, which results in volatilization of OC in the sample. Then the temperature rises and the punch is reheated stepwise to near 900 ℃ in oxygen-containning atmosphere (usually 2% oxygen and 98% helium)

to burn out all carbon remained (BC). The carbon released from each temperature plateau is converted to methane and measured by a flame ionization detector. Due to the influence of dust on quantitative of BC and OC in snow when using a thermal optical method (Wang et al., 2012), we modified the method that in 100% helium atmosphere, only a temperature plateau (550 ℃) was arranged to reduce the time of that BC was exposed in catalysing atmosphere (Yang et al., 2015). Under ideal conditions, minimum determine limits of total carbon is 0.93 μg C cm^{-2}, with a range of 0.2-750 μg C cm^{-2}. During experiments, the filter blank was 1.23±0.38 μg C cm^{-2}.

To identify uncertainty stemming from instrumental instability and uneven distribution of carbon particles in filters, duplicates of ~30 % of the samples were separately analyzed, with consistent results (BC r^2=0.95, OC r^2=0.87, dust r^2=0.90). Because we analyzed the filters through which melted snow samples passed, the OC measured in our study was water-insoluble OC.

2.4 Footprint analysis

To determine the potential origins of the LAIs deposited on the snow cover, back trajectory analyses were performed using European Centre for Medium-Range Weather Forecasts (ECMWF) analysis fields with the Lagrangian analysis tool LAGRANTO (Sprenger and Wernli, 2015), launched every six hours for six selected sampling sites (including three sites of MYL, NMC, and SETP in the region I, two sites of TGL and NETP in the region II, and LHG in the region III) during the sampling periods. The ECMWF fields (horizontal and vertical wind components) were retrieved on 137 model levels and then interpolated onto a 0.25 °×0.25 °latitude-longitude grid. The FINN v1.5 global fire emission inventory in 2013, speciated with the GEOS-chem mechanism (Wiedinmyer et al., 2011), was used to estimate contributions of open burning-sourced BC at the six selected sites. To estimate whether an air parcel at the measurement site is or not influenced by BC emissions, we calculated the BC emission data along the backward trajectories.

2.5 Albedo measurements and simulations

FieldSpec 4 instrument has 3 nm spectral resolution on the visible/near infrared detector (350–1050 nm, silicon photodiode array), and 10–12 nm resolution on the short-wave infrared detectors (900–2500 nm, InGaAs). Measurements are made by standing “down-sun” of the receptor and taking consecutive scans of downwelling and upwelling radiation. Albedo was measured at two sites (24K and MD in Table S1) with FieldSpec 4 when the weather was clear. These measurements were necessary for comparison to simulated albedos.

Albedo reduction caused by LAIs is calculated by the SNow ICe and Aerosol Radiation (SNICAR) model (Flanner et al., 2007), which utilizes the two-stream radiative transfer solution of Toon et al. (1989) and has been widely used in Arctic snow (e.g., Doherty et al., 2010; Flanner et al., 2007, 2009; Hadley and Kirchstetter, 2012). This simulator provides hemispheric reflectance (albedo) of snow for unique combinations of impurity content (black carbon, dust, and volcanic ash), snow grain size, and incident solar flux characteristics. The input fields include incident radiation, solar zenith angle, surface spectral distribution, effective snow grain radius, snow cover thickness and density, albedo of the underlying ground, and concentrations of impurities. Based on our observations, the effective snow grain radius ranged from 118 to 1774 μm for

different snow samples, and snow density ranged from 150 to 400 kg m^{-3}. These two factors varied in low, medium, and high scenarios in the model runs (Table 1).

In terms of the albedo calculation, RF due to BC and dust can be obtained by using Eq. (1) (Kaspari et al., 2014; Yang et al., 2015):

$$RF = \sum_{0.325\ \mu m}^{2.505\ \mu m} E(\lambda, \theta)\ (\alpha_{(r,\lambda)} - \alpha_{(r,\lambda,imp)})\Delta\lambda \quad (1)$$

where, α is the modeled snow spectral albedo with or without the impurities (imp) of BC and/or dust; E is the spectral irradiance; r is the snow optical grain size; λ is wavelength (μm); and θ is the solar zenith angle for irradiance.

2.6 Estimates of changes in snow cover duration

To estimate snow melt due to BC and dust, a model was constructed in which the absorptivity of the snow was multiplied by the daily average incoming short-wave radiation (Schmale et al., 2017) from the automatic weather stations (AWS) set up at the meteorological stations near the sampling sites. Factors derived from meteorological stations in the adjacent areas included daily temperature and daily solar short-wave insolation. Average albedo reductions for snow cover by BC and MD were derived from the SNICAR model. To calculate the amount of snow melted based on the enthalpy of fusion of water (334 J g^{-1}), the snow cover was assumed to be at 0 ℃ and then snowmelt was calculated by using Eq. (2) (Schmale et al., 2017):

$$\mathrm{Melt}_{snow} = \mathrm{N}_{Tht0} \times \Delta\alpha \times SW \quad (2)$$

where, N_{Tht0} is the number of days with temperature greater than 0 ℃; Δα is the albedo reduction (for clean snow, or caused by BC and dust); and *SW* is the short-wave radiation. From Eq. (2), we can estimate changes of snow cover duration (ΔD) based on the already observed/assumed snow depth. We expressed the results for each case were expressed as low, medium, and high scenarios, based on albedo variations.

3 Results and discussion

3.1 Distributions of LAIs

Across the TP, most samples we took were older wind-packed snow. Generally, the ground layer of snow was usually depth hoar, similar to that in Arctic snow (Doherty et al., 2010) and central North America snow (Doherty et al., 2014). For many of these sampling sites, snow cover was intermittent (Fig. S1). During winter season, surface soil can be carried aloft by strong winds and deposited on snow cover, which affects the concentrations of LAIs (Wang et al., 2013). Our results indicated that spatial distributions of BC, OC, and dust in snow over the TP generally ranged from 202–17468 ng g^{-1}, 491–13880 ng g^{-1}, and 22–846 μg g^{-1}, respectively (Fig. 2). Variations in the concentrations of LAIs were higher in the central to northern TP (Region II and III) than that in the southern TP (Region I) (Table 2). The highest concentrations may be related to the lower snow depth and dirtier snow that resulted from post-deposition processes (e.g., snow at some sites was melting.). In the Region I, the snow was cleaner and had lower concentrations of LAIs that were comparable to concentrations in the old snow of glaciers (Kaspari et al., 2014).

The previous studies also examined the concentrations of LAIs in snow from central North America (Doherty et al., 2014; Skiles and Painter, 2016; Zatko et al., 2016), northern China (Huang et al., 2011; Wang et al., 2013; Ye et al., 2012) , Japan (Kuchiki et al., 2015), Europe (Chýlek et al., 1987), Arctic (Doherty et al., 2010; Forsström et al., 2013), Greenland (Aoki et al., 2014; Zatko et al., 2013), and Antarctic (Warren and Clark, 1990; Zatko et al., 2013). Concentrations of BC and other water-insoluble LAIs from the TP were most similar to those in the snow from northern China (Wang et al., 2013), but higher than those from the Himalayas (Lim et al., 2014). In comparison (Table 2), the LAIs in sow cover of TP showed larger values attributed to the more biomass and/or fossil fuel burning and/or dust deposition from nearby region around the TP (e.g., South Asia, East Asia, and/or western China) (Li et al., 2016; Lu et al., 2012; Ramanathan andCarmichael, 2008).

Ratios of OC to BC (OC/BC) can be used to represent possible emission sources of biomass burning in previous studies (e.g., Bond et al., 2013; Cong et al., 2015). The OC/BC ratio in our sampled surface snow ranged from 0.64 to 3.31 over the TP, generally decreasing from south to north (Fig. 2d). Average ratios for Region I, II, and III were 1.82, 1.31, and 1.14, respectively (Table 2), indicating a decreasing contributions of biomass-sourced aerosols deposition in snow over the TP. The higher OC/BC in region I may be due to its proximity to South Asia combustion sources dominated by biomass burnings (Cong et al., 2015; Li et al., 2016). For example in the LHG region, lower LAI concentrations in fresh clean snow were observed at LHG3 and LHG6 (Fig. 3), while near the glacier at LHG1 and LHG2, the collected wind packed, aged snow samples were quite dirty, and had higher LAI concentrations (Fig. S2a,b, and c). Meanwhile, OC/BC ratios were lower at sites near the glacier (Fig. S2d), implying predominantly non-biomass sourced combustion. Higher ratio of OC/BC were found at the sites near human settlements (LHG7–10) (Fig. S2d), where there was extensive biofuel combustion (e.g., yak dung or straw burning). Because of the variations in sampling periods, snow types and depths, sources of dust and carbonaceous aerosol deposition, and/or strong winds, these results were expected to vary with large uncertainties. In general, however, anthropogenic activities play an important role on the ratios of OC/BC in snow cover.

Figure 3 shows the footprint analyses arrived for selected sites across the TP in winter. The northern TP sites (LHG and NETP) are influenced mainly by air masses from Central Asia and partly by air masses from Euro-Asia, which are similar to sources of dust reaching to the TP (e.g., Zhang et al., 2016). These results are also consistent with those of He et al. (2014), Kopacz et al. (2011), and Lu et al. (2012), who modelled contributions of BC emissions in the same region. In the central (TGL and NMC) and southern region (MYL and SETP) of the TP, air masses originate mainly from Central and South Asia. Anthropogenic BC emissions dominate the BC snow albedo as shown in previous studies (Li et al., 2016; Lu et al., 2012). Open burning-sourced BC contributions decrease from the southern to the northern TP (Fig. 4). In the Himalayan region, open burning-sourced BC accounts for half of the BC deposition on snow cover, reflecting the regions' proximity to large sources in South Asia. In the central TP, open burning-sourced BC accounts for approximately 30 % of the total BC, less than that from aerosol and glacier snow, maybe lack of biofuel contributions. While in the northern TP, anthropogenic BC emissions (more than 70 %) dominate the contribution of BC albedo reduction. Li et al. (2016), using $\Delta^{14}C/\delta^{13}C$ compositions of BC isolated from aerosol and snowpit samples in the TP, also found equal contributions from biomass and fossil fuel combustion in Himalayan region (near the southern TP); whereas BC in the remote northern TP predominantly

derives from fossil fuel combustion (66±16 %). These differences can also be seen from the BC emissions which arrived at the selected sites based on BC inventory data for the year of 2013 (PKU-BC-2013, Wang et al., 2014) in Figure S3. In the southern TP, the amount of BC deposition is larger than that in the northern TP due to influence of BC sources in the south Asia.

3.2 Impacts of LAIs on albedo reduction and radiative forcing

To simulate albedo change and surface RF from BC and dust in snow cover, the multi-layer SNICAR model were used (Flanner et al., 2007). Effective snow grain size and snow density was considered at low, medium, and high scenarios (Table 1) and the SNICAR model was run for all-sky conditions on the specific sampling days (Table S2).

SNICAR model simulated albedo (caused by BC and dust with effective snow grain effective radius=150 μm) matches observed reflectance in both visible and absorptive near-infrared (Fig. 5). The BC strongly reduces visible reflectance (in particular, from 350–800 nm), but has negligible influence at wavelengths beyond 1 μm, since the impact of snow grain size is large in this wavelength range (Flanner et al., 2007; Gardner and Sharp, 2010). The presence of MD also decreases the albedo in the visible wavelength, which is in agreement with a study of the impact of MD on snow radiative properties conducted in the European Alps (Mauro et al., 2015). The deviation between measured and simulated reflectance by MD may be a result of the upper boundary of the SNICAR model in particle dimension. The broadband albedo is comparable to albedo simulated for the wavelength from 350–2500 nm, with albedo differences less than 0.0058 (~2.3 %) (Table 3). For the same wavelengths (350–2500 nm), albedo between measurements and simulations differs less than 0.0155 (~4 %) (Table 3). This result is important, showing that the SNICAR model simulations can represent albedo changes of snow cover in the Third Pole region.

For different scenarios defined by effective snow grain size and snow density in Table 1, clean snow albedos resulting from snow aging range from 0.5992 to 0.7751 (Table 4). If BC or MD were the only impurity in the snow cover, contributions to albedo reduction can reach approximately 37 % or 15 %, respectively, with associated larger RF due to BC. On average, BC and MD contribute albedo reduction at approximately 0.18±0.01 and 0.06±0.004, respectively (Fig. 6). The total albedo reduction contributed by BC and MD is about 38%, with associated RF of 18–32 W m^{-2} (Fig. 6). This highlights the importance of LAIs in snow when testing regional- to global-scale models.

Large uncertainties exist in the estimation of BC snow albedo forcing over the TP. Simulation results using the Community Atmosphere Model version 3.1 showed that the aerosol-induced snow albedo perturbations generate surface radiative flux changes of 5–25W m^{-2} in spring (Qian et al., 2011). Using the SNICAR model coupled a general circulation model, Flanner et al. (2007) showed that, during some spring months, snow-only forcing exceeded 10 and 20 W m^{-2} over parts of the TP. RF in the snow-covered regions due to BC by GEOS-Chem model induced the snow-albedo effect to vary from 5–15W m^{-2} over the TP, an order of magnitude larger than RF as a result of the direct effect (Kopacz et al., 2011). Recently, simulation results (using a global chemical transport model in conjunction with a stochastic snow model and a radiative transfer model) showed annual mean BC snow albedo forcing to be 2.9 W m^{-2} averaged over snow-covered plateau regions, which is a

factor of three larger than the value over global land snow cover (He et al., 2014). Surface RF (simulated by a regional climate model coupled with an aerosol–snow/ice feedback module) induced by dust-in-snow showed positive values in the range of 0–6 W m^{-2} over the interior of the TP, the Himalayas, Pamir, and Tienshan Mountains (Ji et al., 2016b). BC-in-snow/ice can cause positive surface RF (3.0–4.5 W m^{-2}) over the western TP in the monsoon season, with the maximum RF (5–6 W m^{-2}) simulated in the Himalayas and southeastern TP in the non-monsoon season (Ji et al., 2016a). Limited measurements of LAIs in snow cover over the TP have hindered a more robust estimate of forcing by BC and dust-in snow in this region (Bond et al., 2013; Qian et al., 2015). The mean forcing of BC and MD in snow in our study is a little higher than previous results from snowpits (e.g., Ming et al., 2009) and comparable to some parts of TP in spring (20 W^{-2}) (Flanner et al., 2007), which indicates more frequent impurity measurements in terms of different years and locations over the TP are necessary for model validation.

Light-absorbing OC in atmospheric aerosols has various origins, e.g., soil humics, humic-like substances (HULIS), tarry materials from combustion, bioaerosols, etc. (Andreae and Gelenscér, 2006). Chemical and optical properties of OC may differ due to the nature of the OC source or atmospheric processing (Chen and Bond, 2010). In contrast and in comparison to black carbon and mineral dust, the optical properties of OC in snow/ice have hardly been examined. Due to the lack of reliable OC optical properties that span the dimensions of snow grain size and OC particle size, the SNICAR model currently does not support the calculation of OC-in-snow forcing in the same way as that for BC. Thus, in this study, we didn't state the effect of OC on albedo reduction and RF.

3.3 Changes in snow cover duration

Changes of snow cover duration are calculated using a model documented by Schmale et al. (2017) (section 2.6). Short-wave radiation input data (three scenarios defined as 220, 270, and 310 W m^{-2}) were obtained using automatic weather wtation observation data near the sampling sites (Table S3). Snow depth water equivalent (SD mm) was assumed from previous studies in this region (Che et al., 2012; Zhong et al., 2016). In general, the reduction days in snow cover duration is larger for low scenarios than for medium and high scenarios (Fig. 7 and Table 5), particularly when *SW* input data is lower (220 W m^{-2}). If SD was 40 mm, average snow cover duration would be reduced by 1.26±0.05 days (*SW*=310 W m^{-2}) to 1.77±0.07 days (SW=220 W m^{-2}) by BC and dust (Fig. 7a, c, and e). If SD was 100 mm, average snow cover duration would be reduced by 3.14±0.13 days to 4.43±0.18 days from the effect of BC and MD, with a maximum of approximately 9.4 days (Fig. 7b, d, and f). SD plays an import role in the reduction of snow cover duration by LAIs. For different scenarios, MD contributes only about 1 day to the reduction of snow cover duration (Fig. 8 and Table 5). These results imply that reduction in snow cover duration related to LAIs is due mainly to BC. Note that no significant differences in reductions of snow cover duration are found across the Third Pole region (Fig. S3).

Against the background of climate change, changes in duration of snow cover have important consequences for surface energy and water budgets over a range of scales, as well as for cryospheric ecosystems (e.g., Euskirchen et al., 2007; Yuan et al., 2016; Zeeman et al., 2017). Based on measurements and modelling, several studies have documented recent trends toward

accelerated snowmelt and changes in snow cover duration caused by BC and MD across the Himalayan-TP in response to enhanced albedo reduction (Ménégoz et al., 2014; Menon et al., 2010; Xu et al., 2009). Ji et al. (2016a, 2016b) noted that BC and MD in snow/ice decreases surface albedo and causes the snow water equivalent to decrease by 5–25 mm over the TP. Ménégoz et al. (2014) has estimated that both dry and wet BC depositions affect the snow cover, reducing its annual duration by 1 to 8 days, which may potentially influence sustaining seasonal water availability (Immerzeel et al., 2010; Tahir et al., 2015).

3.4 Implications and limitations to snow cover and glaciers over the TP

Based on simulations of albedo reduction and RF, we calculated their effect on snow cover duration on a range of simplistic assumptions. We did not consider meteorological conditions, including clouds, precipitation, etc. Snow metamorphism was also not considered, and in the simulation, snow grains were assumed to be spherical, as previous studies (Flanner et al., 2007; Ginot et al., 2013; Schmale et al., 2017). We also did not consider the BC morphology and its mixing state, and light-absorbing properties of OC and MD, which may also significantly affect the light absorption in the simulation (Andreae and Gelencsér, 2006; Kaspari et al., 2014; Mauro et al., 2015; Painter et al., 2010; Schmale et al., 2017). However, the results presented in this study are deduced from the difference between the solar radiation budget for clean snow and LAI-contaminated snow, for which these assumptions are not critical.

Snow cover duarations derease as estimated in this study, and glaciers over western China have been undergoing extensive recession, with an estimated loss of about ~450 km^3 w.e. in volume and 10% reduction in area during the last 40 years (Yao et al., 2012b). Recently, the annual mass budget of glaciers over the TP is estimated at approximately 15–20 Gt yr^{-1} based on GRACE and ICESat (Gardner et al., 2013; Neckel et al., 2014). These melt waters may affect water resources and social development in surrounding areas, e.g. India and China (Immerzeel et al., 2010).

Total amount of glacier snowmelt caused by LAIs is estimated over the whole TP using the model described in Sec. 2.6. Number of days with average temperature larger than 0 ℃ was assumed to be 70 days (±25%) based on the observations during the melting season. Thus, based on the daily snowmelt (0.76±0.40, 0.67±0.36, and 0.54±0.28 cm w.e. d^{-1} for *SW* at 220, 270, and 310 W m^{-2}, respectively) caused by BC and MD in this study, the estimation shows that approximately 4.61±2.49 Gt yr^{-1} (range of 3.80±1.97 to 5.36±2.78 Gt yr^{-1}) of snowmelt water has been lost due to the effect of BC and MD in snow (Fig. 8). This indicates that glacial snowmelt caused by LAIs contributes ~20 % of total mass balance, and that BC and MD may play an important role in recent accelerated snow and glacial melt. However, this result has large uncertainties associated with the lack of sufficient *in-situ* and distributed observations of spectral albedo, concentrations of LAIs, and coincident changes in snow depth, snow water equivalent, and glacier mass estimates, as discussed by many previous studies (e.g., Ginot et al., 2014; Ménégoz et al., 2014; Qian et al., 2015; Schmale et al., 2017). Nevertheless, the method provides a theoretical approach for evaluating how the presence of LAIs affects the lower parts of the glacier subjected to summer melt.

Our study confirms that BC and other water-insoluble LAIs in snow on land and ice can accelerate the snow aging process, and further reduces snow albedo, and increases the speed of snow cover melt (e.g., Flanner et al., 2007; Mauro et al., 2015;

Painter et al., 2007; Qian et al., 2015). Thus, the impacts of BC and other LAIs need to be properly accounted for regional climate projections in future, particularly in the high-altitude cryosphere. It is also important to note that, without large scale, *in-situ* observation data applied to calibrate BC forcing to constrain simulated values, the impact of BC and other LAIs on the albedo feedback would have been marginal. Schmale et al. (2017) points out that, due to the decreasing trend of dust emissions in Central Asia (Xi and Sokolik, 2015), MD may become less important, while BC deposition may increase as a result of projected increased emissions (Wang et al., 2014). Constraints on BC sources/deposition and climatic/hydrological effects will provide guidance for effective mitigation actions.

4 Conclusions

This study was a large area survey of snow cover over the TP across regions with different climatology and sources of LAIs. Systematically higher values of snow BC concentrations were observed in the central to northern TP (Regions II and III) than that in the southern TP (Region I). This may be related to shallower snow depsths and dirtier snow in Regions II and III as a result of post-deposition processes (e.g., snowdrift, or melting). In the southern TP (Region I), the collected snow was cleaner with lower concentrations of LAIs comparable to concentrations in the old glacial snow. The ratios of OC/BC in the surface snow samples ranged from 0.64 to 3.31 across the TP, generally decreasing from south to north TP, which may indicate that anthropogenic activities played an important role on OC/BC ratios in snow cover in the TP region. Footprint analysis also indicated that fossil fuel and biofuel sourced BC accounted for approximately 70 % of total BC deposition in the central and northern TP. Estimates of albedo reduction contributed by BC and MD were approximately 38%, with an associated RF of 18–32 W m^{-2}.

Reported changes in snow cover duration across the TP region relied on single site observations rather than a large area survey. For different scenarios, the reduction in snow cover duration related to LAIs was due mainly to BC, which reduced several days to more than one week. MD contributes only about 1 day to the reduction of snow cover duration. No significant differences among reductions in snow cover duration were found across the TP region. The changing snow cover duration may potentially influence seasonal water availability and sustainability.

Furthermore, the effects of BC and dust on glacier and snowmelt across the TP was estimated based on the simulations of albedo reduction and RF. It was found that glacier snowmelt water caused by LAIs contributed ~20 % of the total mass balance. These findings revealed that effects of both BC and non-BC absorbers effects need to be properly accounted for in future regional climate projections, in particular on the high-altitude cryosphere.

Data availability

Black carbon and other light absorbing data are available upon request from Professor Shichang Kang and Dr. Yulan Zhang.

Author contribution

Y. Zhang, S. Kang, and Z. Cong designed the experiments. M. Sprenger performed the footprint simulations. Y. Zhang, T. Gao, C. Li, X. Li, X. Zhong, and M. Xu, carried the experiments out. S. Tao and W. Meng analysed black carbon inventory. M. Sillanpää gave valuable comments. Y. Zhang prepared the manuscript with contributions from all co-authors.

Acknowledgement

We acknowledge the support provided by the National Natural Science Foundation of China (41630754, 41671067, and 41421061), State Key Laboratory of Cryospheric Sciences (SKLCS-ZZ-2017), Chinese Academy of Sciences (KJZD-EW-G03-04), the Foundation for Excellent Youth Scholars of the Northwest Institute of Eco-Environment and Resources, CAS, and China Scholarship Council. We also thank Dr. M Flanner's help to simulate refelctnce by SNICAR model, and the reviewers who help to the improvement of this manuscript.

References

Andreae, M. O., and Gelencsér, A.: Black carbon or brown carbon? The nature of light-absorbing carbonaceous aerosols, Atmos. Chem. Phys., 6, 3131–3148, 2006.

Aoki, T., Matoba, S., Yamaguchi, S., Tanikawa, T., Niwano, M., Kuchiki, K., Adachi, K., Uetake, J., Motoyama, H., Hori, M.: Light-absorbing snow impurity concentrations measured on Northwest Greenland ice sheet in 2011 and 2012, Bull. Galciol. Res., 32, 21-31, doi:10.5331/bgr.32.21, 2014.

Bahadur, R., Praveen, P.S., Xu, Y., Ramanathan, V.: Solar absorption by elemental and brown carbon determined from spectral observation, Proc. Natl Acad. Sci. USA, 109(43), 17366–17371, doi: 10.1073/pnas.1205910109, 2012.

Beniston, M., Farinotti, D., Stoffel, M., Andreassen, L. M., Coppola, E., Eckert, N., Fantini, A., Giacona, F., Hauck, C., Huss, M., Huwald, H., Lehning, M., López-Moreno, J.-I., Magnusson, J., Marty, C., Moran-Tejéda, E., Morin, S., Naaim, M., Provenzale, A., Rabatel, A., Six, D., Stötter, J., Strasser, U., Terzago, S., Vincent, C.: The European mountain cryosphere: A review of past, current and future issues, Cryosphere Discuss., doi:10.5194/tc-2016-290, 2017.

Bond, T. C., Doherty, S. J., Fahey, D. W., Forster, P. M., Berntsen, T., DeAngelo, B. J., Flanner, M. G., Ghan, S., Kärcher, B., Koch, D., Kinne, S., Kondo, Y., Quinn, P. K., Sarofim, M. C., Schultz, M. G., Schultz, M., Venkataraman, C., Zhang, H., Zhang, S., Bellouin, N., Guttikunda, S.K., Hopke, P. K., Jacobson, M. Z., Kaiser, J. W., Klimont, Z., Lohmann, U., Schwarz, J. P., Shindell, D., Storelvmo, T., Warren, S. G., Zender, C. S.: Bounding the role of black carbon in the climate system: A scientific assessment, J. Geophys. Res. Atmos., 118, 5380–5552, doi:10.1002/jgrd.50171, 2013.

Brown, R. D. and Mote, P. W.: The response of northern Hemisphere snow cover ot a changing climate, J. Clim., 22, 2124–2145, doi: 10.1175/2008JCLI2665.5, 2009.

Cao, J., Lee, S. C., Ho, K. F., Zhang, X., Zou, S. C., Fung, K., Chow, J. C., Watson, J. G.: Characteristics of carbonaceous aerosol in Pearl River Delta Region, China during 2001 winter period, Atmos. Environ., 37:1451–1460, 2003.

Che, T., Dai, L., Wang, J., Zhao, K., Liu, Q.: Estimation of snow depth and snow water equivalent distribution using airborne microwave radiometry in the Binggou Watershed, the uppwe reaches of the Heihe River basin, Int. J. Appl. Earth Obs. Info., 17, 23–32, doi:10.1016/j.jag.2011.10.014, 2012.

Chen, Y., and Bond, T.: Light absorption by organic carbon from wood combustion, Atmos. Chem. Phys., 10, 1773–1787, 2010.

Cheng, G. and Wu, T.: Responses of permafrost to climate change and their environmental significance, Qianhai-Tibet Plateau, J. Geophys. Res. Earth Surface, doi:10.1029/2006JF000631, 2007.

Chow, J. C., Watson, J. G., Chen, L.-W.A., Arnott, W.P., Moosmuller, H., Fung, K. K.: Equivalence of elemental carbon by Thermal/Optical Reflectance and Trsmittance with different temperature protocols, Environ. Sci. Technol., 38(16), 4414-4422, 2004.

Chýlek, P., Srivastava, V., Cahenzli, L., Pinnick, R. G., Dod, R. L., Novakov, T., Cook, T. L., Hinds, B. D.: Aerosol and graphitic carbon content of snow, J. Geophys. Res., 92, 9801-9809, 1987.

Cong, Z., Penetration of biomass-burning emissions from South Asia through the Himalayas: new insights from organic acids, Sci. Rep., 5, 9580, doi:10.1038/srep09580, 2015.

Dang, C., Hegg, A.: Quantifying light absorption by organic carbon in Western North American snow by serial chemical extractions, J. Geophys. Res. Atmos., 119, 10247-10261, doi:10.1002/2014JD022156, 2014.

Doherty, S. J., Dang, C., Hegg, D. A., Zhang, R., Warren, S. G.: Black carbon and other light-absorbing particles in snow of central North America, J. Geophys. Res. Atmos., 119, 12807-12831, doi:10.1002/2014JD022350, 2014.

Doherty, S. J., Warren, S. G., Grenfell, T. C., Clarke, A. D., Brandt, R. E.: Light-absorbing impurities in Arctic snow, Atmos. Chem. Phys., 10, 11647-11680, doi:10.5194/acp-10-11647-2010, 2010.

Dumont, M., Brun, E., Picard, G., Libios, Q., Petit, J.-R., Geyer, M., Morin, S., Josse, B.: Contribution of light-absorbing impurities in snow to Greenland's darkening since 2009, Nat. Geosci., 7, doi:10.1038/NGEO2180, 2014.

Euskirchen, E. S., McGuire, A. D., Chapin III, F. S.: Energy feedbacks of northern high-latitude ecosystems to the climate system due to reduced snow cover during 20th century warming, Global Change Biol., 13, 2425-2438, doi:10.1111/j.1365-2486.2007.01450.x, 2007.

Flanner, M. G., Zender, C. S., Hess, P. G., Mahowald, N. M., Painter, T. H., Ramanathan, V., Rasch, P. J.: Springtime warming and reduced snow cover from carbonaceous particles, Atmos. Chem. Phys., 9, 2481–2497, 2009.

Flanner, M. G., Zender, C. S., Randerson, J. T., Rasch, P. J: Present-day climate forcing and response from black carbon in snow. J. Geophys. Res., 112, D11202, 2007.

Flanner, M. G.: Arctic climate sensitivity to local black carbon, J. Geophys. Res. Atmos., 118, 1840-1851, doi:10.1002/jgrd.50176, 2013.

Forsström, S., Isaksson, E., Skeie, R. B., Strom, J., Pedersen, C.A., Hudson, S.R., Berntsen, T. K., Lihavainen, H., Godtliebsen, F., Gerland, S.: Elemental carbon measurements in European Arctic snow packs, J. Geophys. Res. Atmos., 118, 13614–13627, doi:10.1002/2013JD019886, 2013

Gabbi, J., Huss, M., Bauder, A., Cao, F., Schwiowski, M.: The impact of Saharan dust and black carbon on albedo and long-term mass balance of an Alpine glacier, Cryosphere, 9, 1385-1400, 2015.

Gardner, A. S., Moholdt, G., Cogley, J. G., Wouters, B., Arendt, A. A., Wahr, J., Berthier, E., Hock, R., Pfeffer, W. T., Kaser, G., Ligtenberg, S. R. M., Bolch, T., Sharp, M. J., Hagen, J. O., van den Broeke, M. R., Paul, F.: A reconciled estimate of glacier contributions to sea level rise: 2003 to 2009, Science, 340, 852-858, 2013.

Gardner, A. S. and Sharp, M. J.: A review of snow and ice albedo and the development of a new physically based broadband albedo parameterization, J. Geophys. Res., 115, F01009, doi:10.1029/2009JF001444, 2010.

Gertler, C. G., Puppala, S. P., Panday, A., Stumm, D., Shea, J.: Black carbon and the Himalayan cryosphere: A review, Atom. Environ., 125, 404-417, doi: 10.1016/j.atmosenv.2015.08.078, 2016.

Ginot, P., Dumont, M., Lim, S., Patris, N., Taupin, J.-D., Wagnon, P., Gilbert, A., Arnaud, Y., Marinoni, A., Bonasoni, P., Laj, P.: A 10 year record of black carbon and dust from a Mera Peak ice core (Nepal): variability and potential impact on melting of Himalayan glaciers, Cryosphere, 8, 1479-1496, doi:10.5194/tc-8-1479-2014, 2014.

Hadley, O. L., Kirchstetter, T. W.: Black-carbon reduction of snow albedo, Nat. Clim. Chan., 2, doi:10.1038/NCLIMATE1433, 2012.

Hansen, J. and Nazarenko, L.: Soot climate forcing via snow and ice albedos, Proc. Natl Acad. Sci. USA, 101, 423–428, 2004.

He, C., Liou, K.-N., Takano, Y., Gu, Y., Qi, L., Mao, Y., Leung, L. R.: Black carbon radiative forcing over the Tibetan Plateau, Geophys. Res. Lett., 41, 7806–7813, doi:10.1029/2014GL062191, 2014.

Huang, J., Fu, Q., Zhang, W., Wang, X., Zhang, R., Ye, H., Warren, S. G.: Dust and black carbon in seasonal snow across northern China, BAMS, doi:10.1175/2010BAMS3064.1, 2011.

Immerzeel, W. W., van Beek, L. P. H., Bierkens, M. F. P.: Climate change will affect the Asian water towers, Science, 328, 1382–1385, 2010.

Jacobi, H.-W., Lim, S., Ménégoz, M., Ginot, P., Laj, P., Bonasoni, P., Stocchi, P., Marinponi, A., Araud, Y.: Black carbon in snow in the upper Himalayan Khumbu Valley, Nepal: observation and modelling of the impact on snow albedo, melting, and radiative forcing, Cryoshere, 9, 1385-1400, doi:10.5194-tc-1385-2015, 2015.

Ji, Z., Kang, S., Cong, Z., Zhang, Q., Yao, T.: Simulation of carbonaceous aerosols over the Third Pole and adjacent regions: distribution, transportation, deposition, and climatic effects, Clim. Dyn., doi:10.1007/s00382-015-2509-1, 2015.

Ji, Z., Kang, S., Zhang, Q., Cong, Z., Chen, P., Sillanpää, M.: Investigation of mineral aerosols radiative effects over Hihg Mountain Asia in 1990-2009 using a regional climate model, Atmos. Res., 178–179, 484–496, doi: 10.1016/j.atmosres.2016.05.003, 2016a.

Ji, Z.: Modeling black carbon and its potential radiative effects over the Tibetan Plateau, Adv. Clim. Change Res., 7, 139-144, 2016b.

Kang, S., Xu, Y., You, Q., Flühel, W.-A., Pepin, N., Yao, T.: Review of climate and cryosphere change in the Tibetan Plateau, Environ. Res. Lett., 5, 015101, doi:10.1088/1748-9326/5/1/015101, 2010.

Kaspari, S., Painter, T. H., Gysel, M., Skiles, S. M., Schwikowski, M.: Seasonal and elevational variations of black carbon and dust in snow and ice in the Solu-Khumbu, Nepal and estimated radiative forcings, Atmos. Chem. Phys., 14, 8089–8103, 2014.

Kopacz, M., Mauzerall, D. L., Wang, J., Leibensperger, E. M., Henze, D. K., Singh, K.: Origin and radiative forcing of black carbon transported to the Himalayas and Tibetan Plateau, Atmos. Chem. Phys., 11, 2837–2852, doi:10.5194/acp-11-2837-2011, 2011.

Kuchiki, K., Aoki, T., Niwano, M., Matoba, S., Kodama, Y., Adachi, K.: Elemental carbon, organic carbon, and dust concentrations in snow measured with thermal optical and gravimetric methods: Variations during the 2007-2013 winters at Sapporo, Japan, J. Geophys. Res. Atmos., 120, 868-882, doi:10.1002/2014JD022144, 2015.

Lau, W. K. M., Kim, M.-K., Kim, K.-M., Lee, W.-S.: Enhanced surface warming and accelerated snow melt in the Himalayas and Tibetan Plateau induced by absorbing aerosols, Environ. Res. Lett., 5, 025204, doi:10.1088/1748-9326/5/2/025204, 2010.

Li, C., Bosch, C., Kang, S., Andersson, A., Chen, P., Zhang, Q., Cong, Z., Chen, B., Qin, D., Gustafsson, Ö.: Sources of black carbon to the Himalayan-Tibetan Plateau glaciers, Nat. Comm., 7, 12574, doi:10.1038/ncomms12574, 2016.

Li, X., Kang, S., He, X., Qu, B., Tripathee, L., Jing, Z., Paudyal, R., Li, Y., Zhang, Y., Yan, F., Li, G., Li, C.: Light-absorbing impurities accelerate glacier melt in the Central Tibetan Plateau, Sci. Total Environ., doi:10.1016/j.scitotenv.2017.02.169, 2017.

Lin, G., Penner, J. E., Flanner, M. G., Sillman, S., Xu, L., Zhou, C.: radiative forcing of organic aerosol in the atmosphere and on snow: Effects of SOA and brown carbon, J. Geophys. Res. Atmos., 119, 7453-7476, doi:10.1002/2013JD021186, 2014.

Lu, Z., Streets, D. G., Zhang, Q., Wang, S.: A novel back-tracjectory analysis of the origin of black carbon transported to the Himalayas and Tibetan Plateau during 1996–2010, Geophys. Res. Lett., 39(L01809), doi:10.1029/2011GL049903, 2012.

Mauro, B. D., Fava, F., Ferrero, L., Garzonio, R., Baccolo, G., Delmonte, B., Colombo, R.: Mineral dust impact on snow radiative properties in the European Alps combining ground, UAV, and satellite observations, J. Geophys. Res. Atmos., 120, 6080–6097, doi:10.1002/2015JD023287, 2015.

Ménégoz, M., Krinner, G., Balkanski, Y., Boucher, O., Cozic, A., Lim, S., Ginot, P., Laj, P., Gallée, H., Wagnon, P., Marinoni, A., Jacobi, H. W.: Snow cover sensitivity to black carbon deposition in the Himalayas: from atmospheric and ice core measurements to regional climate simulations, Atmos. Chem. Phys., 14, 4237-4249, doi:10.5194/acp-14-4237-2014, 2014.

Menon, S., Koch, D., Beig, G., Shu, S., Fasullo, J., Orlikowski, D.: Black carbon aerosol and the third polar ice cap, Atmos. Chem. Phys., 10, 4559–4571, doi:10.5194/acp-10-4559-2010, 2010.

Ming, J., Xiao, C., Cachier, H., Qin, D., Qin, X., Li, Z., Pu, J.: Black carbon (BC) in the snow of glaciers in west China and its potential effects on albedos, Atmos. Res., 92, 114-123, doi: 10.1016/j.atmosres.2008.09.007, 2009.

Nechel, N., Kropáček, J., Bolch, T., Hochschild, V.: Glacier mass changes on the Tibetan Plateau 2003-2009 derived from ICESat laser altimetry measurements, Environ. Res. Lett., 9(1), 014009, doi: 10.1088/1748-9326/9/1/014009, 2014.

Niu, H., Kang, S., Shi, X., Paudyal, R., He, Y., Li, G., Wang, S., Pu, T., Shi, X.: In-situ measurements of light-absorbing impurities in snow of glacier on Mt. Yulong and implications for radiative forcing estimates, Sci. Total Environ., doi: 10.1016/j.scitotenv.2017.01.032, 2017.

Painter, T. H., Barrett, A. P., Landry, C. C., Neff, J. C., Cassidy, M. P., Lawrence, C. R., McBride, K. E., Farmer, G. L.: Impact of disturebed desert soils on duration of mountain snow cover, Geophys. Res. Lett., 34, L12502, doi:10.1029/2007GL030284, 2007.

Painter, T. H., Deems, J. S., Belnap, A. F., Landry, C. C., Udall, B.: Response of Colorado River runoff to dust radiative forcing in snow, Proc. Natl. Acad. Sci. USA, 107(40), 17125-17130, doi:10.1073/pnas.0913139107, 2010.

Painter, T. H., Seidel, F. C., Bryant, A. C., Skiles, S. M., Rittger, K.: Imaging spectroscopy of albedo and radiative forcing by light-absorbing impurities in mountain snow, J. Geophys. Res. Atmos., 118, 9511-9523, doi:10.1002/jgrd.50520, 2013.

Pu, Z., Xu, L., Salomonson, V. V.: MODIS/Terra observed seasonal variations of snow cover over the Tibetan Plateau, Geophys. Res. Lett., 34(L06706), doi:10.1029/2007GL029262, 2007.

Qian, Y., Flanner, M. G., Leung, L. R., Wang, W.: Sensitivity studies on the impacts of Tibetan Plateau snowpack pollution on the Asian hydrological cycle and monsoon climate, Atmos. Chem. Phys., 11, 1929–1948, doi:10.5194/acp-11-1929-2011, 2011.

Qian, Y., Wang, H., Zhang, R., Flanner, M. G., Rasch, P. J.: A sensitivity study on modelling black carbon in snow and its radiative forcing over the Arctic and northern China, Eviron. Res. Lett., 9, 064001, doi:10.1088/1748-9326/9/6/064001, 2014.

Qian, Y., Yasunari, T. J., Doherty, S. J., Flanner, M. G., Lau, W. K. M., Ming, J., Wang, H., Wang, M., Warren, S. G., Zhang, R.: Light-absorbing particles in snow and ice: measurement and modeling of climatic and hydrological impact, Adv. Atmos. Sci., 32, 64–91, doi: 10.1007/s00376-014-0010-0, 2015.

Qu, B., Ming, J., Kang, S., Zhang, G., Li Y., Li, C., Zhao, S., Ji, Z. and Cao, J.: The decreasing albedo of the Zhadang glacier on western Nyainqengtanglha and the role of light-absorbing impurities, Atmos. Chem. Phys., 14, 11117–11128, doi:10.5194/acp-14-11117-2014, 2014.

Ramanathan, V. and Carmichael, G.: Global and regional climate changes due to black carbon, Nat. Geosci., 1, 221-227, doi:10.1038/nego156, 2008.

Schmale, J., Flanner, M., Kang, S., Sprenger, M., Zhang, Q., Guo, J., Li, Y., Schwikowski, M., Farinotti, D.: Modulation of snow reflectance and snowmelt from Central Asian glaciers by anthropogenic black carbon, Sci. Rep., 7, 40501, doi:10.1038/srep40501, 2017.

Skiles, S. M. and Painter, T. H.: Daily evolution in dust and black carbon content, snow grain size, and snow albedo during snowmelt, Rocky Mountains, Colorado, J. Glaciol., doi:10.1017/jog.2016.125, 2016.

Skiles, S. M., Painter, T. H., Belnap, J., Holland, L., Reynolds, R. L., Goldstein, H. L., Lin, J.: Regional variability in dust-on-snow processes and impacts in the Upper Colorado River basin, Hydrol. Process., doi:10.1002/hyp.10569, 2015.

Sprenger, M., and Wernli, H.: The LAGRANTO Lagrangian analysis tool–version 2.0, Geosci. Model Dev., 8, 2569–2586, doi: 10.5194/gmd-8-2569-2015, 2015.

Tahir, A. A., Chevallier, P., Arnaud, Y., Ashraf, M., Bhatti, M. T.: Snow cover trend and hydrological characteristics of the Astore River basin (Western Himalayas) and its comparison to the Hunza basin (Karakoram region), Sci. Total Environ., 505, 748–761, doi: 10.1016/j.scitotenv.2014.10.065, 2015.

Toon, O. B., McKay, C. P., Ackerman, T. P., Santhanam, K.: Rapid calculation of radiative heating rates and photodissociation rates in inhomogeneous multiple scattering atmospheres, J. Geophys. Res. Atmos., 94(D13), 16287–16301, 1989.

Vernek, A. D., Zhou, J., Shukla, J.: The effect of Eurasian snow cover on the Indian Monsoon, J. Clim., 8, 248–266, 1995.

Wang, M., Xu, B., Zhao, H., Cao, J., Joswiak, D., Wu, G., Lin, S.: The influence of dust on quantitative measurements of black carbon in ice and snow when using a thermal optical method, Aerosol Sci. Tech., 46:1, 60–69, doi:10.1080/02786826.2011.605815, 2012.

Wang, R., Tao, S., Shen, H., Huang, Y., Chen, H., Baljanski, Y., Boucher, O., Ciais, P., Shen, G., Li, W., Zhang, Y., Chen, Y., Lin, N., Su, S., Li, B., Liu, J., Liu, W.: Trend in black carbon emissions from 1960 to 2007, Environ. Sci. Technol., doi:10.1021/es5021422, 2014.

Wang, X., Doherty, S., Huang, J.: Black carbon and other light-absorbing impurities in snow across Northern China, J. Geophys. Res. Atmos., 118, 1471-1492, doi:10.1029/2012JD018291, 2013.

Warren, S. G., Clarke, A. D.: Soot in the atmosphere and snow surface of Antarctica, J. Geophys. Res., 95(D2), 1811-1816, 1990.

Wiedinmyer, C., Akagi, S. K., Yokelson, R. J., Emmons, L. K., Al-Saadi, J. A.: The Fire Inventory from NCAR (FINN): A high resolution global model to estimate the emissions from open burning, Geosci. Model Dev., 4, 625-641, doi:10.5194/gmd-4-625-2011, 2011.

Xi, X. and Sokolik, I. N.: Dust interannual variability and trend in Central Asia from 2000 to 2014, and their climatic linkages, J. Geophys. Res. Atmos., 120, 12175–12197, doi:10.1002/2015JD024092, 2015.

Xu, B., Cao, J., Hansen, J., Yao, T., Joswia, D. R., Wang, N., Wu, G., Wang, M., Zhao, H., Yang, W., Liu, X., He, J.: Black soot and the survival of Tibetan glaciers, Proc. Natl. Acad. Sci. U.S.A., 106 (52), 22114–22118, doi:10.1073/pnas.0910444106, 2009.

Yanai, M. and Wu, G.: Effects of the Tibetan Plateau, in B. Wang (ed.) The Asian Monsoon, Springer Berlin Heidelberg, 513-549, 2006.

Yang, S., Xu, B., Cao, J., Zender, C. S., Wang, M.: Climate effect of black carbon aerosol in a Tibetan Plateau glacier, Atmos. Environ., 111, 71-78, doi:10.1016/j.atmosenv.2015.03.016, 2015.

Yao, T., Masson-Delmotte, V., Gao, J., Yu, W., Yang, X., Risi, C., Sturm, C., Werner, M., Zhao, H., He, Y., Ren, W., Tian, L., Shi, C., Hou, S.: A review of climatic controls on $\delta^{18}O$ in precipitation over the Tibetan Plateau: Observations and simulations, Rev. Geophys., 51, doi:8755-1209/13/10.1002/rog.20023, 2013.

Yao, T., Thompson, L.G., Mosbrugger, V., Zhang, F., Ma, Y., Luo, T., Xu, B., Yang, X., Joswiak, D. R., Wang, W., Joswiak, M. E., Devkota, L. P., Tayal, S., Jilani, R., Fayziev, R.: Third Pole Environment (TPE), Environ. Development, 3, 52–64, doi: 10.1016/j.envdev.2012.04.002, 2012a.

Yao, T., Thompson, L.G., Yang, W., Yu, W., Gao, Y., Guo, X., Yang, X., Duan, K., Zhao, H., Xu, B., Pu, J., Lu, A., Xiang, Y., Kattel, D.B., Joswiak, D.: Different glacier status with circulations in TP and surroundings, Nat. Clim. Change, doi: 10.1038/NCLIMATE1580, 2012b.

Yasunari, T. J., Bonasoni, P., Laj, P., Fujita, K., Vuillermoz, E., Marinoni, A., Cristofanelli, P., Duchi, R., Tartari, G., Lau, K.-M.: Estimated impact of black carbon deposition during pre-monsoon season from Nepal Climate Observatory- Pyramid data and snow albedo changes over Himalayn glacier, Atmos. Chem. Phys., 10, 6603–6615, doi:10.5194/acp-10-6603-2010, 2010

Yasunari, T. J., Koster, R. D., Lau, Kim, K.-M.: Impact of snow darkening via dust, black carbon, and organic carbon on boreal spring climate in the Earth system, J. Geophys. Res. Atmos., 120, 5485-5503, doi:10.1002/2014JD022977, 2015.

Yasunari, T. J.,Tan, Q., Lau, K.-M., Bonasoni, P., Marinoni, A., Laj, P., Ménégoz, M., Takemura, T., Chin, M.: Estimated range of black carbon dry deposition and the related snow albedo reduction over Himalayan glaciers during dry pre-monsoon periods, Atom. Environ., 78, 259-267, doi: 10.1016/j.atmosenv.2012.03.031, 2013.

Ye, H., Zhang, R., Shi, J., Huang, J., Warren, S. G., Fu, Q.: Black carbon in seasonal snow across northern Xinjiang in northwestern China, Environ. Res. Lett., 7, 044002, doi:10.1088/1748-9326/7/4/04002, 2012.

Yuan, W., Xu, W., Ma, M., Chen, S., Liu, W., Cui, L.: Improved snow cover model in terrestrial ecosystem models over the Qinghai-Tibetan Plateau, Agr. Forest Meterol., 218–219, 161–170, doi: 10.1016/j.agrformet.2015.12.004, 2016.

Zatko, M. C., Grenfell, T. C., Alexander, B., Doherty, S. J., Thomas, J. L., Yang, X.: The influence of snow grain size and impurities on the vertical profiles of actinic flux and associated NOx emission on the Antarctic and Greenland ice sheets, Atmos. Chem. Phys., 13, 3547-3567, doi:10.5194/acp-13-3547-2013, 2013.

Zatko, M. C., Erbland, J., Savarino, J., Geng, L., Easley, L., Schauer, A. J., Bates, T. S., Quinn, P., Light, B., Morison, D., Osthoff, H. D., Lyman, S., Neff, W., Yuan, B., Alexander, B.: The magnitude of the snow-sourced reactive nitrogen flux to the boundary layer in the Uintah Basin, Utah, USA, Atmos. Chem. Phys., 16, 13537-13851, doi:10.5194/acp-16-13837, 2016.

Zeeman, M. J., Mauder, M., Steinbrecher, R., heidbach, K., Echart, E., Schmid, H. P.: Reduced snow cover ffects productivity of upland temperate grasslands, Agr. Forest Meterol., 232, 514–526, doi: 10.1016/j.agrformet.2016.09.002, 2017.

Zhang, R., Wang, H., Qian, Y., Rasch, P. J., Easter, R. C., Ma, P.-L., Singh, B., Huang, J., Fu, Q.: Quantifying sources, transport, deposition, and radiative forcing of black carbon over the Himalayas and Tibetan Plateau, Atmos. Chem. Phys., 15, 6205-6223, doi:10.5194/acp-15-6205-2015, 2015.

Zhang, Y., Kang, S., Zhang, Q., Gao, T., Guo, J., Grigholm, B., Huang, J., Sillanpää, M., Li, X., Du, W., Li, Y., Ge, X.: Chemical records in snowpits from high altitude glaciers in the Tibetan Plateau and its surroundings, PLoS ONE, 11(5), e0155232, doi:10.1371/journal.pone.0155232, 2016.

Zhang, Y., Li, T., Wang, B.: Decadal change of the spring snow depth over the Tibetan Plateau: The associated circulation and influence on the east Asian summer monsoon, J. Clim., 17, 2780-2793, 2004.

The Cryosphere Discuss., https://doi.org/10.5194/tc-2017-111
Manuscript under review for journal The Cryosphere
Discussion started: 14 July 2017

Zhong, X., Zhang, T., Zheng, L., Hu, Y., Wang, H., Kang, S.: Spatiotemporal variability of snow depth across the Eurasian continent from 1966 to 2012, Cryosphere Discuss., doi:10.5194/tc-2016-182, 2016.

The Cryosphere Discuss., https://doi.org/10.5194/tc-2017-111
Manuscript under review for journal The Cryosphere
Discussion started: 14 July 2017

Table 1 Snow effective grain sizes and snow density used for the albedo calculation with the SNICAR model.

Description	Low scenario	Central scenario	High scenario
Snow effective grain radius (μm)	150	500	1500
Snow density (kg m^{-3})	150	250	400

Table 2 Summary of BC, OC and dust concentrations in snow over the Third pole region and other regions.

Sites	BC (ng g^{-1})	Dust (μg g^{-1})	OC (ng g^{-1})	OC/BC	Method	References
Southern TP (Region I)	1423±242	119.8±18.97	2145±325	1.82±0.17	DRI	This study
Central TP (Region II)	5624±1500	295±67.50	6119±1257	1.31±0.19	DRI	This study
Northern TP (Region III)	1484±626	93.20±27.05	974±197	1.14±0.15	DRI	This study
Himalayan Khumbu Valley	0.1-70				SP2	Jacobi et al., 2015
Himalayas	24.3±20.1	1.32±0.84	359±185.2	~10	Sunset	Lim et al., 2014
Qilian mountain	1550				ISSW	Wang et al., 2013
Border of Siberia, China	117				ISSW	Wang et al., 2013
Northeast China	1220				ISSW	Wang et al., 2013
Inner Mongolia, China	340				ISSW	Wang et al., 2013
Northwest China	10-150				ISSW	Pu et al., 2016
Sapporo, Japan	7-2800	10-1300	0.14-260		Sunset	Kuchiki et al., 2015
Central North America	5-70				ISSW	Doherty et al., 2014
Uintah basin, Utah, USA	5-100				ISSW	Zatko et al., 2016
Sierra Nevada, North America	11±7.7				DRI	Hadley et al., 2010
French Alps	4.3±4.5	3.06±5.25	59.6±77.6		SP2	Lim et al., 2014
Greenland Summit	3.1±1.4	0.262±0.117	142.6±82.6		SP2	Lim et al., 2014
Greenland	Sumit station: 1.4				ISSW	Zatko et al., 2013
Arctic	Scandinavia: 88 Svalbard: 11-14 Fram Strait: 7-42 Barrow: 9				Sunset	Forsström et al., 2013
Antarctic	Near Dome C: 2.1 Far from Dome C: 0.6				ISSW	Zatko et al., 2013

Note:

(1) DRI-DRI 2001A model thermal-optical carbon analysis
(2) SP2: Single Particle Soot Photometer
(3) ISSW- ISSW spectrophotometer
(4) Sunset: Sunset Lab OC-EC Aerosol Analyzer

The Cryosphere Discuss., https://doi.org/10.5194/tc-2017-111
Manuscript under review for journal The Cryosphere
Discussion started: 14 July 2017

Table 3 Comparison between measured albedo by ASD and simulated albedo (SA) by SNICAR model.

Selected site (24K)	SA clean snow	SA BC	SA Dust	SA BC+Dust
SNICAR: Broadband (305-4495 nm)	0.7824	0.7027	0.7511	0.6892
SNICAR: Wavelength (350-2500 nm)	0.7728	0.6985	0.7453	0.6864
ASD measurement (350-2500 nm)		0.6709±0.0019		

Table 4 Simulated albedo (SA) and radiative forcing (RF) by BC and dust in snow cover across the Third Pole region.

Different scenarios	SA clean snow	SA BC	SA Dust	SA BC+Dust	Contribution to albedo reduction	RF BC	RF Dust	RF BC+Dust
Low	0.7751±0.0193	0.6517±0.0702	0.7387±0.0250	0.6413±0.0710	37%	16.32±0.0931	4.78±0.0310	17.64±0.0952
Medium	0.6943±0.0313	0.5104±0.0900	0.6372±0.0382	0.4992±0.0900	39%	24.20±0.1250	7.57±0.0483	25.86±0.1233
High	0.5992±0.0435	0.3683±0.0935	0.5197±0.0490	0.3582±0.0889	38%	30.96±0.1362	10.70±0.0653	32.36±0.1315

Table 5 Average reductions of snow cover duration by BC and dust for different shortwave (220, 270, and 310 W m-2, respectively) and snow cover depth water equivalent (mm).

SD / Shortwave	SD=40 mm			SD=100 mm		
	BC	Dust	BC+dust	BC	Dust	BC+dust
SW=220 W m^{-2}	1.69±0.07	0.74±0.04	1.77±0.07	4.24±0.18	1.84±0.10	4.43±0.18
SW=270 W m^{-2}	1.38±0.06	0.60±0.03	1.44±0.06	3.45±0.15	1.50±0.08	3.61±0.15
SW=310 W m^{-2}	1.20±0.05	0.52±0.03	1.26±0.05	3.01±0.13	1.31±0.07	3.14±0.13

The Cryosphere Discuss., https://doi.org/10.5194/tc-2017-111
Manuscript under review for journal The Cryosphere
Discussion started: 14 July 2017

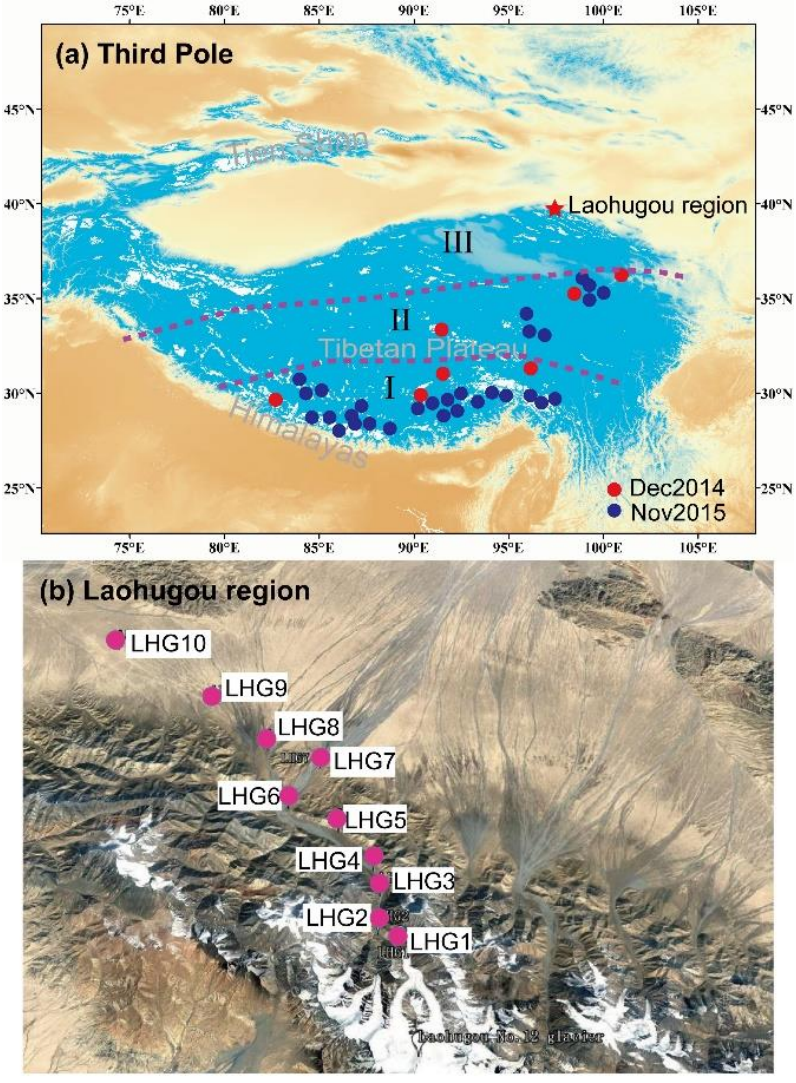

Figure 1: Snow sampling sites over (a) the Third Pole region and (b) the Laohugou region.

The Cryosphere Discuss., https://doi.org/10.5194/tc-2017-111
Manuscript under review for journal The Cryosphere
Discussion started: 14 July 2017

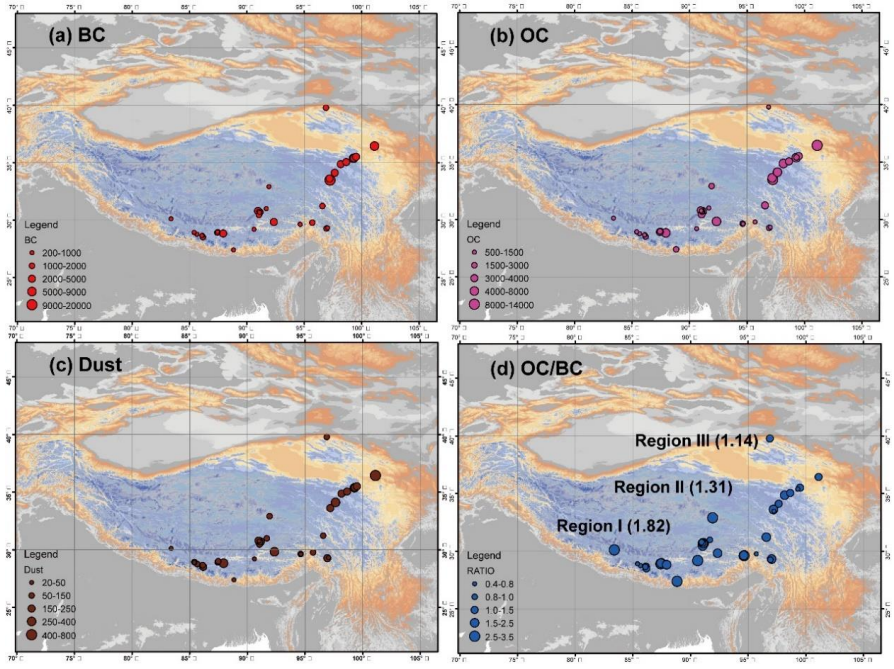

Figure 2: Spatial distributions of light-absorbing impurities for each sampling site over the Third Pole region. (a) BC, (b) OC, (c) Dust, and (d) ratio of OC to BC (OC/BC).

The Cryosphere Discuss., https://doi.org/10.5194/tc-2017-111
Manuscript under review for journal The Cryosphere
Discussion started: 14 July 2017

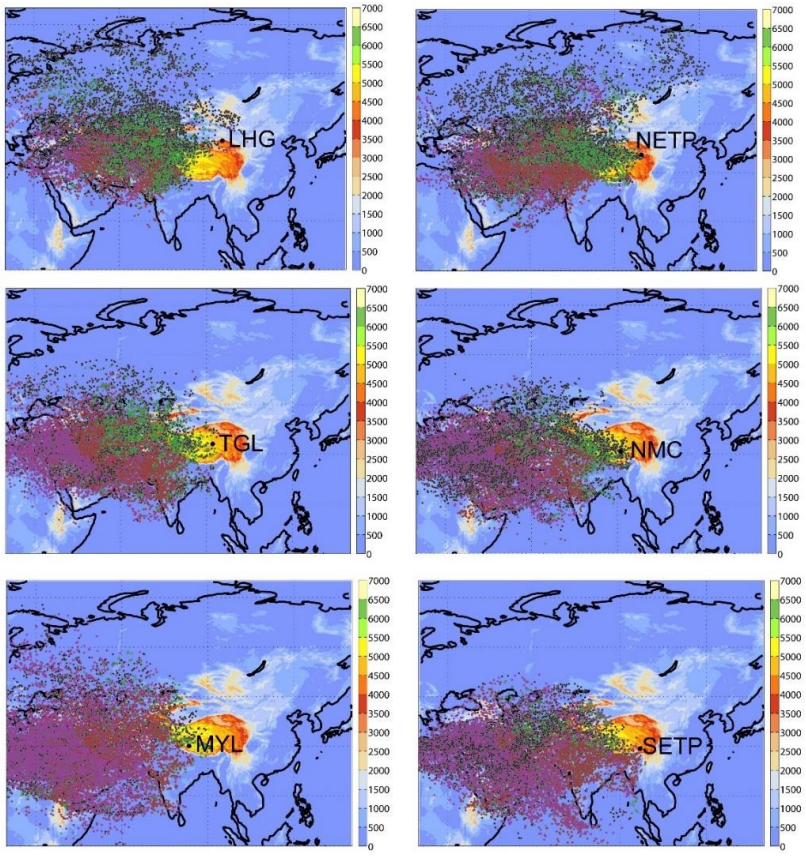

Figure 3: Footprint analyses for selected six sites over the Third Pole region during the winter season (Nov 2015-Feb 2016). LHG and NETP in the northern Tibetan Plateau (Region III), TGL and NMC in the central Tibetan Plateau (Region II), and MYL and SETP in the southern Tibetan Plateau (Region I).

The Cryosphere Discuss., https://doi.org/10.5194/tc-2017-111
Manuscript under review for journal The Cryosphere
Discussion started: 14 July 2017

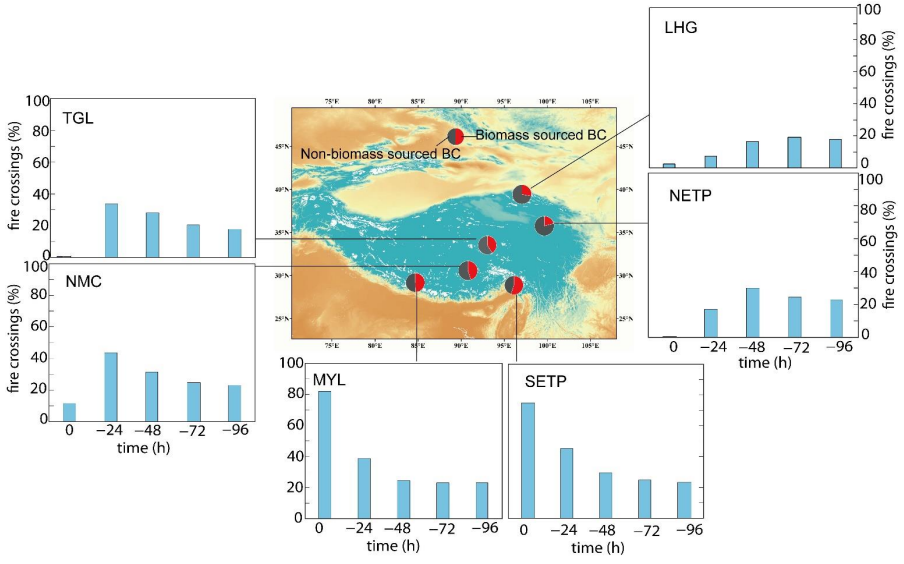

Figure 4: Different source contributions to BC deposition on the snow cover in the Third Pole region.

39

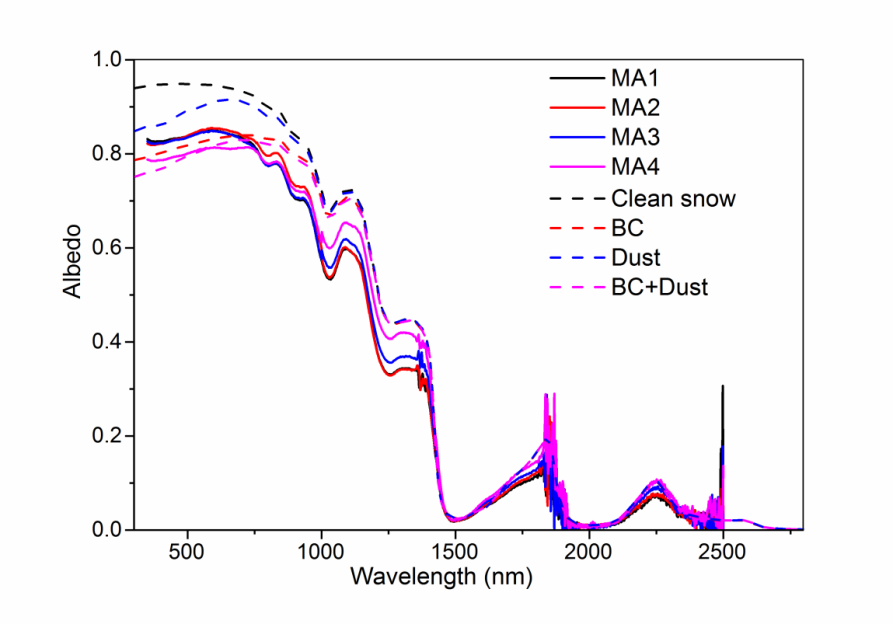

40

41 **Figure 5: Measured albedo (MA1-4) by ASD and effects of BC and dust on albedo at the selected snow site on**
42 **the Third Pole.**

43

The Cryosphere Discuss., https://doi.org/10.5194/tc-2017-111
Manuscript under review for journal The Cryosphere
Discussion started: 14 July 2017

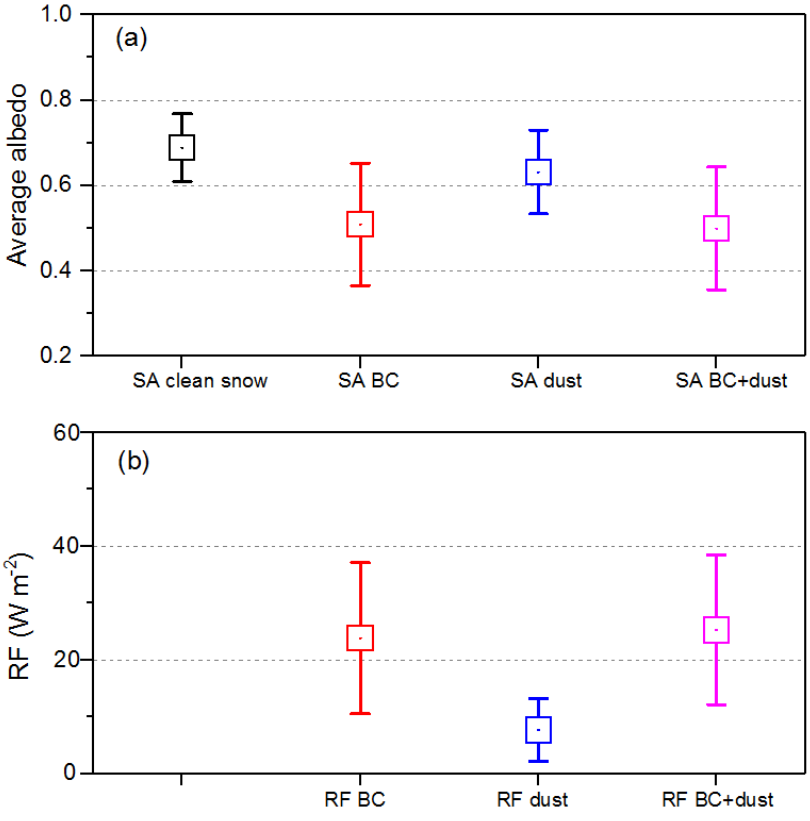

Figure 6: (a) Average albedo of snow cover due to aging only and impurities relative to the clean snow and (b) resulting all sky daily-mean radiative forcing. (Note: SA=simulated albedo; RF=radiative forcing; The rectangles are the central estimate while the bars show the standard deviation range of the snow grain size and snow density scenarios defined in Table1.)

The Cryosphere Discuss., https://doi.org/10.5194/tc-2017-111
Manuscript under review for journal The Cryosphere
Discussion started: 14 July 2017

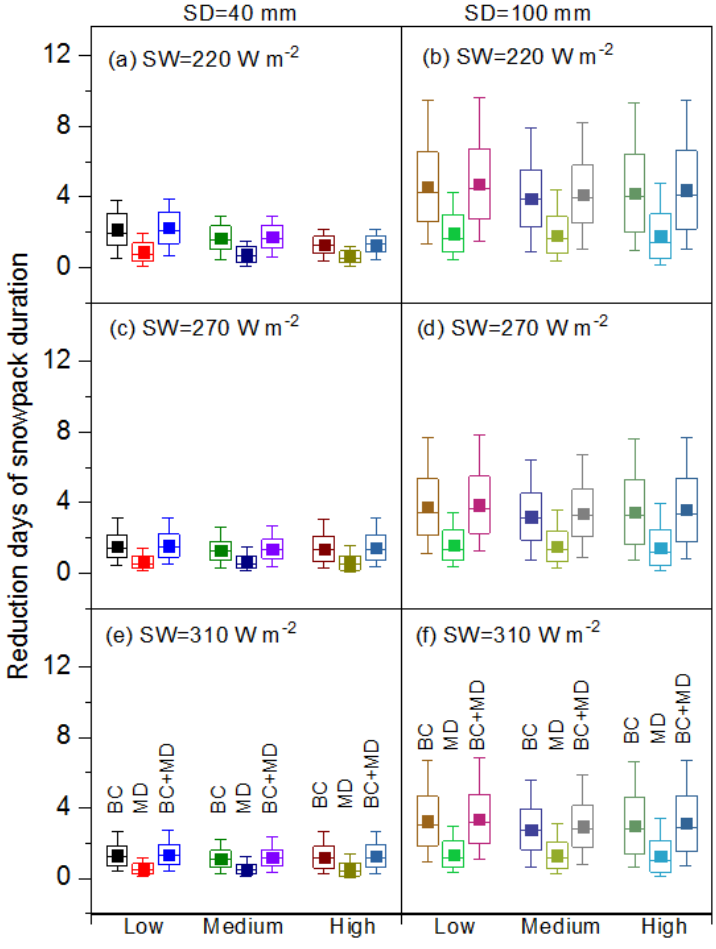

Figure 7: Reduction days of snow cover duration by BC and dust for low, medium and high scenarios due to albedo reduction at different snow depth (SD=40 and 100 mm, respectively), a and b simulated based on the daily shortwave at 220 W m-2, c and d simulated based on the daily shortwave at 270 W m-2, e and f simulated based on the daily shortwave at 310 W m-2. (Solid rectangles are mean values; outliers of boxes are one standard deviations; and bars are maximum and minimum values.)

The Cryosphere Discuss., https://doi.org/10.5194/tc-2017-111
Manuscript under review for journal The Cryosphere
Discussion started: 14 July 2017

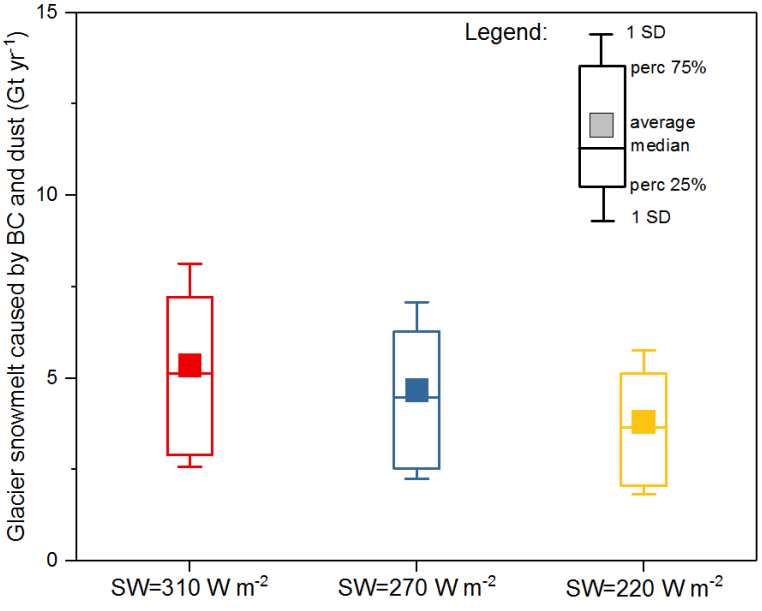

Figure 8: Estimates of total glacier snowmelt based on daily snowmelt caused by BC and dust for shortwave radiation at 220, 270, and 310 W m^{-2}, respectively. Days of daily temperature larger than 0 °C is assumed to be 100 days (±25%).